J|A|C|S
ARTICLES

Published on Web 07/19/2008

Rational Enhancement of Second-Order Nonlinearity: Bis-(4-methoxyphenyl)*hetero*-aryl-amino Donor-Based Chromophores: Design, Synthesis, and Electrooptic Activity

Joshua A. Davies, Arumugasamy Elangovan,* Philip A. Sullivan,* Benjamin C. Olbricht, Denise H. Bale, Todd R. Ewy, Christine M. Isborn, Bruce E. Eichinger, Bruce H. Robinson, Philip J. Reid, Xiaosong Li, and Larry R. Dalton*

Department of Chemistry, University of Washington, 109 Bagley Hall, Box 351700, Seattle, Washington 98195

Received January 29, 2008; E-mail: easamy@u.washington.edu; psull76@u.washington.edu; dalton@chem.washington.edu

Abstract: Two new highly hyperpolarizable chromophores, based on *N,N-bis*-(4-methoxyphenyl)*aryl*-amino donors and phenyl-trifluoromethyl-tricyanofuran (**CF_3-Ph-TCF**) acceptor linked together via π-conjugation through 2,5-divinylenethienyl moieties as the bridge, have been designed and synthesized successfully for the first time. The *aryl* moieties on the donor side of the chromophore molecules were varied as to be thiophene and 1-*n*-hexylpyrrole. The linear and nonlinear optical (NLO) properties of all compounds were evaluated in addition to recording relevant thermal and electrochemical data. The properties of the two new molecules were comparatively studied. These results are critically analyzed along with two other compounds, reported earlier from our laboratories and our collaborator's, that contain (i) aliphatic chain-bearing aniline and (ii) dianisylaniline as donors, keeping the bridge (2,5-divinylenethienyl-), and the acceptor (**CF_3-Ph-TCF**), constant. Trends in theoretically (density functional theory, DFT) predicted, zero-frequency gas-phase hyperpolarizability [$\beta(0;0,0)$] values are shown to be consistent with the trends in $\beta_{HRS}(-2\omega;\omega,\omega)$, as measured by Hyper-Rayleigh Scattering (HRS), when corrected to zero-frequency using the two-level model (TLM) approximation. Similarly, trends in poling efficiency data (r_{33}/E_p) and wavelength dispersion measured by reflection ellipsometry (using a Teng−Man apparatus) and attenuated total reflection (ATR) are found to fit the TLM and DFT predictions. A 3-fold enhancement in bulk nonlinearity (r_{33}) is realized as the donor subunits are changed from alkylaniline to dianisylaminopyrrole donors. The results of these studies provide insight into the complicated effects on molecular hyperpolarizability of substituting heteroaromatic subunits into the donor group structures. These studies also demonstrate that, when frequency dependence and electric-field-induced ordering behavior are correctly accounted for, *ab initio* DFT generated $\beta(0;0,0)$ is effective as a predictor of changes in r_{33} behavior based on chromophore structure modification. Thus DFT can provide valuable insight into the electronic structure origin of complex optical phenomena in organic media.

Introduction

Development of highly efficient organic electrooptic (EO) materials has been the focal point of recent research among many organic materials research groups. This research is driven by the attractive potential of improving the efficiency of nonlinear optical (NLO) material while lowering production cost for applications including electrooptic modulation (the Pockels effect), optical rectification, and terahertz radiation generation and detection.[1–4] In order for the material to display very large bulk EO response (characterized by its EO coefficient, r_{33}), noncentrosymmetrically aligned active materials must have large molecular hyperpolarizabilities (β), low optical loss, and excellent thermal-, chemical-, and photochemical stabilities.[5–7]

When considering the design of dipolar π-conjugated chromophores as organic second-order nonlinear optical materials, optimization of electron donor and electron acceptor substituents is necessary to obtain maximum nonlinearity at the molecular level. Moreover, chemical-, photochemical-, and thermal stability in turn depend on the nature of these groups.

In general, dipolar second-order NLO chromophores consist of a π-conjugated bridge end-capped with strong electron donor and acceptor substituents (D−π−A). It is well established that extremely large β values can be achieved by optimizing the ground-state polarization by carefully considering which com-

(1) Baehr-Jones, T.; Hochberg, M.; Wang, G.; Lawson, R.; Liao, Y.; Sullivan, P. A.; Dalton, L.; Jen, A. K. Y.; Scherer, A. *Opt. Express* **2005**, *13*, 5216–5226.
(2) Dalton, L. R. *Adv. Polym. Sci.* **2002**, 158.
(3) Schneider, A.; Guenter, P. *Ferroelectrics* **2005**, *318*, 83–88.
(4) Sinyukov, A. M.; Leahy, M. R.; Hayden, L. M.; Haller, M.; Luo, J.; Jen, A. K. Y.; Dalton, L. R. *Appl. Phys. Lett.* **2004**, *85*, 5827–5829.
(5) He, M.; Leslie, T. M.; Sinicropi, J. A.; Garner, S. M.; Reed, L. D. *Chem. Mater.* **2002**, *14*, 4669–4675.
(6) Marder, S. R.; Kippelen, B.; Jen, A. K. Y.; Peyghammbarian, N. *Nature (London)* **1997**, *388*, 845–851.
(7) Zhang, C.; Dalton, L. R.; Oh, M.-C.; Zhang, H.; Steier, W. H. *Chem. Mater.* **2001**, *13*, 3043–3050.

bination of these three components can be used to impart a necessary directional bias.[8] Several D−π−A systems are known in the literature, and the EO properties of the best of these materials is improved by an order of magnitude as compared to the best known inorganic material, $LiNbO_3$. Yet, the full potential of organic electrooptic materials remains largely unrealized. In order to optimize molecular hyperpolarizability, much effort has been focused on the design and synthesis of optimized conjugated bridge and electron acceptor structures while, in the newest generation of EO chromophores, the donor units have remained relatively unchanged. Building upon this knowledge, we envisaged that a further enhancement of molecular hyperpolarizability could be achieved by introducing stronger electron donors. Unfortunately, the relative inflexibility of the structural make up of the currently available chromophore electron donor units have presented hurdles in this path for achieving durable materials with enhanced electrooptic activity, possessing a balance of all desirable qualities.

Apart from a few recent works,[9,10] very little experimental or theoretical research has been focused on the use of the 4-(diarylamino)*aryl* group as the electron donor in NLO chromophores despite very comparable π-donor strengths with respect to their 4-(dialkylamino)*aryl* analogues, and demonstrated superior thermal stability and photostability.[9,10] Moreover, the π-donor strength of 4-(diarylamino)phenyl moieties can be tuned by the structural variation of the substituents on the aryl rings. Much of the reluctance in incorporating these donors into dipolar chromophores stems from the general lack of success in translating large microscopic hyperpolarizability (β) into large macroscopic EO response (r_{33}), which may be caused by π−π stacking interactions and charge transport between chromophores. Recently, Jen and some of us were able to overcome some of these challenges to achieve an order of magnitude improvement in r_{33} over previous triarylamino chromophores.[9]

Conceptually, a strategy that could be used to increase π-donor strength is to replace the phenyl ring, commonly used in the donor end of the main conjugation, with heteroaromatic molecules having reduced aromaticity and ionization potential.[10] Despite several accounts of experimental and theoretical work suggesting that the use and location of heteroaromatic units may have the potential to dramatically increase β,[10–18] there are very few examples of second-order NLO chromophores making use of di*alkyl*amino-heteroaryl donors,[19–21] and fewer of di*aryl*amino-heteroaryl donors.[22–24] An explanation for this void in the literature probably has to do with the reported difficulty in functionalizing a heteroaromatic ring with an arylamine. Although amination of 2- and 3-halo-thiophene is known,[22–28] Hartwig and co-workers indicated that the reluctance to attempt such reactions with 2- or 3-bromo-pyrroles is owed to the instability of the starting material.[25] In fact, to the best of the authors' knowledge, such an analogous functionalization has not been previously reported.

In this work, aminoheteroarmomatic (thienyl- and pyrrolyl-) groups were explored as a replacement for the phenyl (i.e., aniline) unit in the donor part of the donor-π-acceptor molecule. For this study, two new compounds based on *N,N-bis*-(4-methoxyphenyl)*aryl*-amine donors were synthesized anew. These chromophores contain the key 2,5-divinylthienyl (**FTC**) bridge and the powerful 2-dicyanomethylen-3-cyano-4-methyl-5-phenyl-5-trifluoromethyl-2,5-dihydrofuran (**CF_3-Ph-TCF**) acceptor. The *N,N-bis*-(4-methoxyphenyl)*phenyl*-amino donor-containing chromophore **A** (Chart 1) was chosen as a reference for comparison and further enhancement of β by synthetic modification not only because it has a larger calculated π-donor strength, but it is also experimentally shown to have a 2-fold improvement in molecular hyperpolarizability (β) and a 3-fold macroscopic EO response (r_{33}) over the simple triphenylamino analogue.[9]

The use of complementary experimental and theoretical methods enables us to explore and evaluate the effects of structural modifications in this series of molecules. Density functional theory (DFT) quantum mechanical calculations were used to model ground and exited state electron-density configurations and evaluate the changes in zero-frequency hyperpolarizability, $\beta(0;0,0)$, to be expected with donor group modification. These data were then used in concert with linear optical property measurements to deconvolute the frequency dependence of hyper-Rayleigh scattering (HRS) measurements as well as attenuated total reflection (ATR) measurements of electric field poling-induced r_{33}. In addition to nonlinear optical measurements, relevant linear optical, electrochemical, and thermal properties are reported and discussed herein.

Results and Discussion

Synthesis. The syntheses of donors **5a** and **5b** are outlined in Scheme 1. The literature method for making **5a** involves a two-

(8) Marder, S. R.; Gorman, C. B.; Meyers, F.; Perry, J. W.; Bourhill, G.; Bredas, J.-L.; Pierce, B. M. *Science (Washington)* **1994**, *265*, 632–635.
(9) Cheng, Y.-J.; Luo, J.; Hau, S.; Bale, D. H.; Kim, T.-D.; Shi, Z.; Lao, D. B.; Tucker, N. M.; Tian, Y.; Dalton, L. R.; Reid, P. J.; Jen, A. K. Y. *Chem. Mater.* **2007**, *19*, 1154–1163.
(10) Kwon, O.; Barlow, S.; Odom, S. A.; Beverina, L.; Thompson, N. J.; Zojer, E.; Bredas, J.-L.; Marder, S. R. *J. Phys. Chem. A* **2005**, *109*, 9346–9352.
(11) Albert, I. D. L.; Marks, T. J.; Ratner, M. A. *J. Am. Chem. Soc.* **1997**, *119*, 6575–6582.
(12) Breitung, E. M.; Shu, C.-F.; McMahon, R. J. *J. Am. Chem. Soc.* **2000**, *122*, 1154–1160.
(13) Leclercq, A.; Zojer, E.; Jang, S. H.; Barlow, S.; Geskin, V.; Jen, A. K. Y.; Marder, S. R.; Bredas, J. L. *J. Chem. Phys.* **2006**, *124*, 044510/1−044510/7.
(14) Rao, V. P.; Jen, A. K. Y.; Chandrasekhar, J.; Namboothiri, I. N. N.; Rathna, A. *J. Am. Chem. Soc.* **1996**, *118*, 12443–12448.
(15) Batista, R. M. F.; Costa, S. P. G.; Malheiro, E. L.; Belsley, M.; Raposo, M. M. M. *Tetrahedron* **2007**, *63*, 4258–4265.
(16) Facchetti, A.; Beverina, L.; van der Boom Milko, E.; Dutta, P.; Evmenenko, G.; Shukla, A. D.; Stern, C. E.; Pagani Giorgio, A.; Marks Tobin, J. *J. Am. Chem. Soc.* **2006**, *128*, 2142–21453.
(17) Raposo, M. M. M.; Sousa, A. M. R. C.; Kirsch, G.; Ferreira, F.; Belsley, M.; de Matos Gomes, E.; Fonseca, A. M. C. *Tetrahedron* **2005**, *61*, 11991–11998.
(18) Raposo, M. M. M.; Sousa, A. M. R. C.; Kirsch, G.; Cardoso, P.; Belsley, M.; de Matos Gomes, E.; Fonseca, A. M. C. *Org. Lett.* **2006**, *8*, 3681–3684.
(19) Jen, A. K. Y.; Rao, V. P.; Wong, K. Y.; Drost, K. J. *J. Chem. Soc., Chem. Commun.* **1993**, 90–92.
(20) Rao, V. P.; Cai, Y. M.; Jen, A. K. Y. *J. Chem. Soc., Chem. Commun.* **1994**, 1689–1690.
(21) Rao, V. P.; Jen, A. K. Y.; Wong, K. Y.; Drost, K. J. *Tetrahedron Lett.* **1993**, *34*, 1747–1750.
(22) Bedworth, P. V.; Cai, Y.; Jen, A.; Marder, S. R. *J. Org. Chem.* **1996**, *61*, 2242–2246.
(23) Hu, Z.-Y.; Fort, A.; Barzoukas, M.; Jen, A. K. Y.; Barlow, S.; Marder, S. R. *J. Phys. Chem. B* **2004**, *108*, 8626–8630.
(24) Jen, A. K. Y.; Cai, Y.; Bedworth, P. V.; Marder, S. R. *Adv. Mater.* **1997**, *9*, 132–135.
(25) Hooper, M. W.; Utsunomiya, M.; Hartwig, J. F. *J. Org. Chem.* **2003**, *68*, 2861–2873.
(26) Ogawa, K.; Rasmussen, S. C. *J. Org. Chem.* **2003**, *68*, 2921–2928.
(27) Wu, I.-Y.; Lin, J. T.; Tao, Y.-T.; Balasubramaniam, E.; Su, Y. Z.; Ko, C.-W. *Chem. Mater.* **2001**, *13*, 2626–2631.
(28) Yamashita, M.; Hartwig, J. F. *J. Am. Chem. Soc.* **2004**, *126*, 5344–5345.

Chart 1. Structures of the Chromophores **YLD156, A**, **B**, and **C**

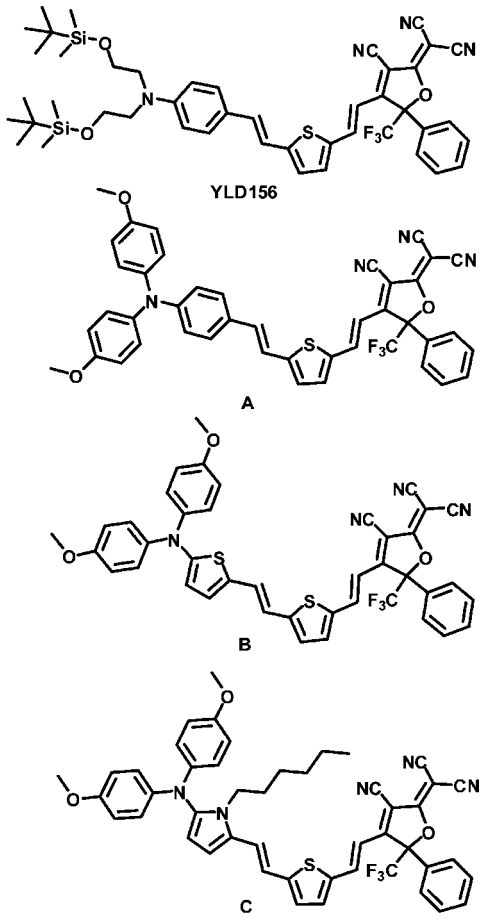

step process wherein 4-bromobenzonitrile is first coupled with 4,4′-dimethoxydiphenylamine using Hartwig−Buchwald palladium-catalyzed amination, then reduced using DIBAL-H to afford **5a** in a 73% yield overall.[9] While this yield is satisfactory, it was improved to 89% and reduced to one step by directly coupling 4,4′-dimethoxydiphenylamine to 4-bromobenzaldehyde. Although donor **5b** is reported in the literature its preparation has yet to be disclosed. It was prepared in a manner analogous to that for **5a** in 60% yield.

The preparation of **5c**, as shown in Scheme 2, was much more challenging and involved several attempts by different routes before the synthesis was satisfactorily completed. To facilitate incorporation of the pyrrole into an NLO chromophore, and to increase solubility, the labile nitrogen proton was replaced with an *n*-hexyl chain following a literature procedure.[29] As shown in Route A, 1-hexyl-1*H*-pyrrole was then monobrominated at the 2 position producing the desired product with good selectivity (90% as determined by ^{1}H NMR). This bromide was then reacted with 4,4′-dimethoxydiphenylamine, following typical Pd-catalyzed coupling procedures, to produce **2** in 85% yield. The instability of the 2-pyrrole-containing compounds, as cited by Hartwig, was realized during the attempted Vilsmeier formylation of **2**, which resulted in decomposition and failed to yield **5c**. After a second attempt at the formylation of **2** using *n*-butyllithium resulted in the same fate, a newly revised plan was followed. As shown in Route B, Scheme 2, 1-hexyl-1*H*-pyrrole was dibrominated selectively and quantitatively using *N*-bromosuccinimide in tetrahydrofuran at −78 °C, then monoformylated with dimethylformamide following lithium exchange at −78 °C using *n*-butyllithium. 5-Bromo-1-hexyl-1*H*-pyrrole-2-carbaldehyde **4** was then aminated with the dianisylamine to produce **5c** in 59% yield over four steps. Thus, we have successfully devised a novel synthetic protocol for the preparation of the previously unknown compound **5c.**

Following the synthetic exploration invested into the preparation of donors **5a**−**5c**, the effort put forth toward the syntheses of chromophores **A**, **B**, and **C**, as outlined in Scheme 3, was more or less the same in comparison to the synthesis of other FTC type chromophores. In a parallel fashion, donors **5a**−**5c** were extended to the donor-bridges **6a**−**6c**, all in 80 to 95% yield, using efficient Horner-Wadsworth-Emmons olefination methodology using diethyl (2-methylthiophene) phosphonate. Donor-bridge intermediates were then formylated in excellent yields at the 5′ position using *n*-butyllithium and DMF at −78 °C. Finally, the Knoevenagel condensation reaction with the **CF_3Ph-TCF** acceptor proceeded smoothly in ethanolic solution in the presence of an inorganic base to give final chromophores **A**, **B**, and **C** in 70−75% yield. Thus, the overall yields of **A**, **B**, and **C** were 51%, 19%, and 34%, respectively.

Linear optical and electrochemical properties. UV−visible absorption spectral and electrochemical methods were employed to explore the differing electron-donating properties provided by the modified donor moieties. The recorded UV−visible absorption spectra of compounds **A**, **B**, **C**, and **YLD156** in chloroform are displayed in Figure 1 and the photophysical and electrochemical data are recorded in Table 1.

When comparing the λ_{max} of *bis*-(4-methoxyphenyl)amino*phenyl* donor-containing chromophore **A** (745 nm) with its dialkylaminophenyl counterpart **YLD156** (753 nm), **A** is slightly blue-shifted and the two compounds exhibit similar charge-transfer band shape.

It may be noted that the presence of the dianisyl group in **A**, **B**, and **C** gives rise to the high-energy band at 500 nm which is absent in **YLD156**. Replacing the phenyl donor group with the thiophene donor, or the *N*′-hexylpyrrole donor, has a profound effect on the charge-transfer bands resulting in 112 nm, and 108 nm, respectively, red-shifted values for chromophores **B** and **C**. While the charge-transfer band of **B** is slightly broader than that of **A**, that of **C** is by far the broadest, particularly the low-energy tail of the transition, which extends all the way out to about 1200 nm. This could indicate that the CT state is populated over a wide range of energy levels, suggesting that the vibrational contribution is disfavored or that the vibrational components are masked under the broad CT band. This can be explained on the basis that the pyrrole moiety, coupled with the strong electron-donating ability of the dianisyl units, augments the electron-donating ability of the donor. The HOMO and LUMO orbitals for structure **C** show that the pyrrole group contributes roughly equally to both, which suggests that it fosters electron transfer from the donor to the bridge (see Figure 2C). Broadening can also be caused by an increased density of states in the excited state. Such a situation can arise from high excitation into the vibrational manifold. This circumstance would require a drastic change in Franck−Condon overlap, suggesting a large geometry change, which would be common for a molecule consisting of a loose, long, and efficient conjugation structure versus a rigid polynuclear aromatic system. In spite of the fact that the charge transfer state is spread over 500 nm, the oscillator strength appears to be satisfactory as

(29) Lion, C.; Baudry, R.; Hedayatullah, M.; Da Conceicao, L.; Hocquaux, M.; Genard, S.; Maignan, J. *J. Heterocycl. Chem.* **2000**, *37*, 1635–1640.

Scheme 1. Syntheses of Donors **5a**, and **5b**[a]

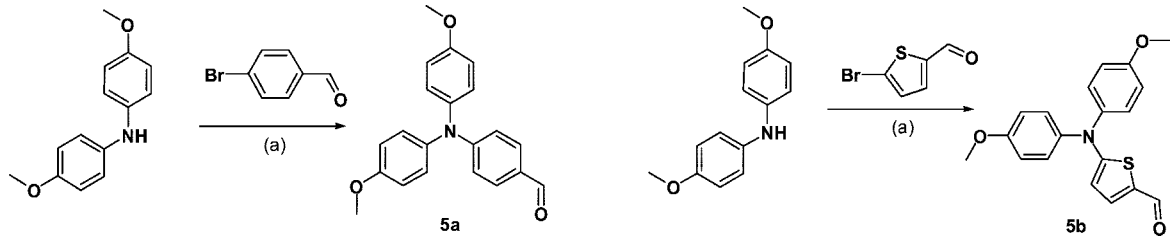

[a] Reagents and conditions: (a) 2 mol % $Pd_2(dba)_3$, 4 mol % $(t\text{-Bu})_3P$, *t*-BuONa, toluene, 125 °C, 18 h.

Scheme 2. Synthesis of Donor **5c**[a]

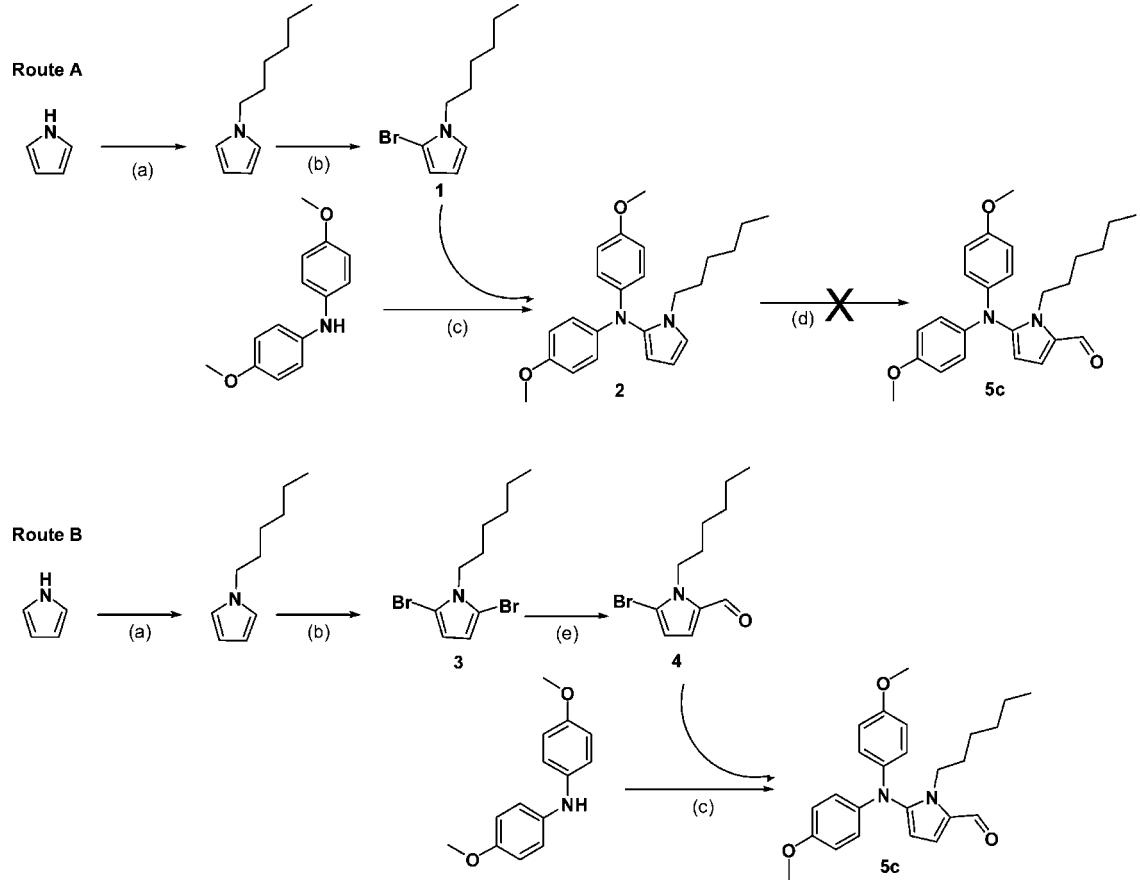

[a] Reagents and conditions: (a) 1-bromo-hexane, NaH, THF, 65 °C, 12 h. (b) NBS, THF, −78 to −15 °C 4 h. (c) 2 mol % $Pd_2(dba)_3$, 4 mol % $(t\text{-Bu})_3P$, *t*-BuONa, toluene, reflux, 18 h. (d) $POCl_3$, DMF, diethylether, 0 °C to rt, 6 h, then 1 N HCl. (e) *n*-BuLi, THF, −78 °C, 1 h, then DMF, −78 °C to rt, 1 N HCl.

compared with the rest of the series as seen from the molar absorptivity in chloroform.

Chromophore **B**, having two thiophene rings in the bridge, exhibits a minor contribution from a vibrational coupling appearing as a slight shoulder at about 800 nm in addition to the major charge transfer band at 857 nm. This shoulder could originate from the fact that, although there is sufficient charge transfer transition possible in this chromophore, the somewhat symmetrical nature of the bridge impacts the molecule to reduce its CT nature, making it a slightly unperturbed system favoring vertical excitation to populate the Franck−Condon state, especially around the bridge units. This is supported by the narrowness of the band structure as well. Additional support for this contention comes from the DFT-calculated HOMO structures (Figure 2), wherein one can see a strong delocalization of both HOMO and LUMO on the dithienylethene bridge.

The UV−vis absorption spectra were also measured in dioxane so that solvatochromic behavior of the chromophores could be explored (Table 1). Compounds **B** and **C** showed very large hypsochromic shifts of 107 and 95 nm, respectively, from chloroform to dioxane, whereas compounds **A** and **YLD156**

(30) Accelrys: San Diego, 2002.
(31) Delley, B. In *Modern Density Functional Theory: A Tool for Chemistry*; Seminario, J. M., Politzer, P. , Eds.; Elsevier Science Publishers: Amsterdam, 1995; Vol. 2.
(32) Hammer, B.; Hansen, L. B.; Norskov, J. K. *Phys. Rev. B: Condens. Mater. Phys.* **1999**, *59*, 7413–7421.
(33) Frisch, M. J.; et al. *Gaussian03*, B.04 ed.; Gaussian, Inc: Wallingford, CT, 2004.
(34) Lee, C.; Yang, W.; Parr, R. G. *Phys. Rev. B: Condens. Mater. Phys.* **1988**, *37*, 785–789.
(35) Hariharan, P. C.; Pople, J. A. *Theor. Chim. Acta* **1973**, *28*, 213–22.
(36) Hehre, W. J.; Ditchfield, R.; Pople, J. A. *J. Chem. Phys.* **1972**, *56*, 2257–2261.

Scheme 3. Syntheses of Chromophores **A**, **B**, and **C**[a]

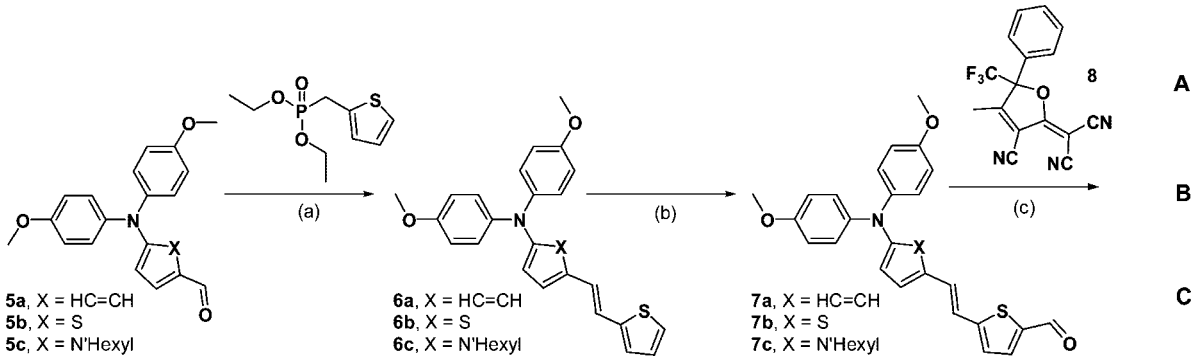

[a] Reagents and conditions: (a) *t*-BuOK, THF, 0 °C to rt, 8 h. (b) *n*-BuLi, THF, −78 °C, 1 h, then DMF, −78 °C to rt, 1 N HCl. (c) CF_3Ph-TCF acceptor (**8**) EtOH, 8 h rt.

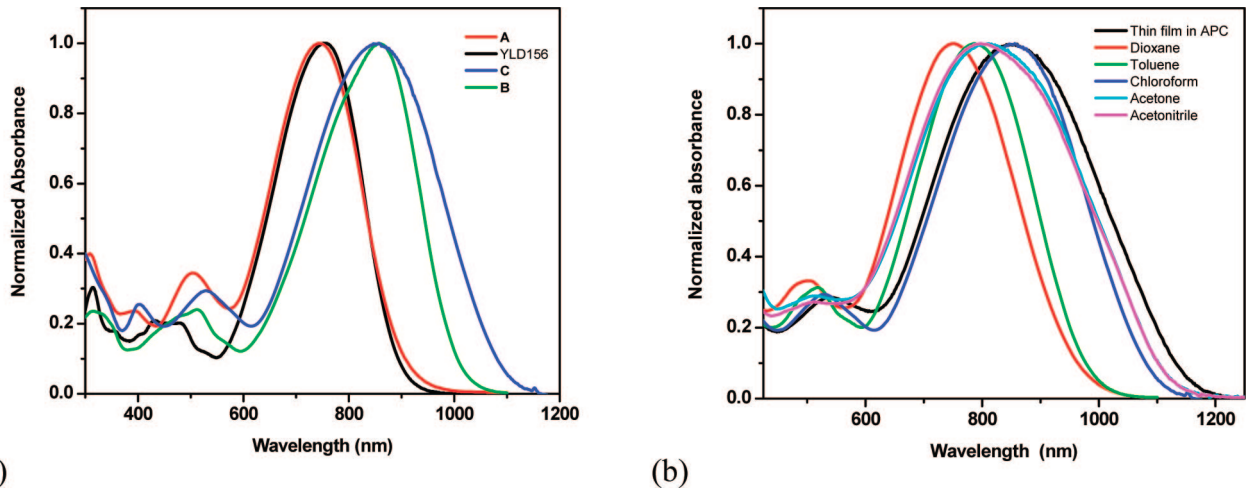

Figure 1. (a) Absorption spectra of chromophores **A**, **B**, **C**, and **YLD156** in chloroform. (b) Solvatochromic behavior of **C** recorded in different solvents of varying dielectric constants (dioxane: 2.25; toluene: 2.38; $CHCl_3$: 4.81; acetone: 20.7; acetonitrile: 37.5) and as film in amorphous polycarbonate (APC). It may be noted that the spectrum recorded for the film (black) appears very similar (with slight broadening) to that recorded in chloroform (blue).

Table 1. Summary of Optical Absorption and Electro-chemical Data

	absorption λ_{max} (nm)			ϵ ($\times 10^4$ M^{-1} cm^{-1})						
cmpd	dioxane	toluene	$CHCl_3$	dioxane	toluene	$CHCl_3$	ΔE (UV)[a] (eV)	E_{ox}[b] (V)	E_{red}[c] (V)	ΔE (CV)[d] (eV)
YLD156	687	710	753	5.64	5.16	6.21	1.38	0.395	−0.815	1.03
A	682	713	745	5.06	3.95	5.10	1.37	0.189	−0.952	0.95
B	750	811	857	5.05	5.41	6.23	1.23	0.174	−0.822	0.84
C	758	786	853	4.37	4.12	4.85	1.09[e]	0.075[c]	−0.824	0.71

[a] Estimated from the onset of the absorption at the low-energy edge in chloroform. [b] Referenced to ferrocene standard ($E_{1/2}$ = 0.39 in CH_2Cl_2). [c] Arrived at using peak potential as the reactions are irreversible. [d] $E_{HOMO} = -e[4.8\ V + (E_{ox\ (onset)} - Fc_{ox\ (onset)})]$; $E_{LUMO} = -e[4.8\ V + (E_{red\ (onset)} - Fc_{red\ (onset)})]$. [e] Estimated from the onset of the absorption at the low-energy edge in solid film in APC.

had moderate blue-shifts of 63 and 66 nm, respectively. An extended solvatochromic study was attempted for **C**; the spectra are overlain in Figure 1b. While the charge transfer band showed decent solvatochromic red-shift upon increasing the solvent dielectric constant, there appears to be a threshold for this behavior for such a highly polarizable compound as **C** that there occurs a reversal of CT upon increasing the dielectric constant to beyond 20.7 [acetone and acetonitrile (37.5) appear to favor excessive charge transfer in this compound] leading to back electron donation causing blue-shift from the absorption in chloroform. This confirms the concept that chromophores **B** and **C** are more strongly polarizable than even **YLD156** and **A**.

In order to determine the electrochemical properties of the compounds under study, cyclic voltammetry (CV) experiments were performed in degassed anhydrous dichloromethane solutions containing Bu_4NPF_6 as the supporting electrolyte. Voltammograms of $\sim 10^{-3}$ M solutions of chromophores **A**, **B**, **C**, and **YLD156** were recorded, and the E_{ox} and E_{red} for each compound, relative to ferrocene standard, were determined from each data set and furnished in Table 1. Cyclic voltammetric traces recorded for all compounds are shown in Figure 3. The one-electron oxidation reaction was found to be typically Nernstian (fully reversible) for **A** and **YLD156**, whereas that for compounds **B** was quasi-reversible and that for **C** was found to be completely irreversible, as was the reduction reaction for all four compounds. The observed electrochemical behavior can be explained by taking into account the orbital structures of the HOMO and LUMO for the compounds studied (Figure 2). In the case of compounds **B** and **C** the transfer of an electron from the donor to the anode occurs adiabatically during the forward scan as the one-electron oxidation. As the potential is switched, the electron added to the molecule probably does not

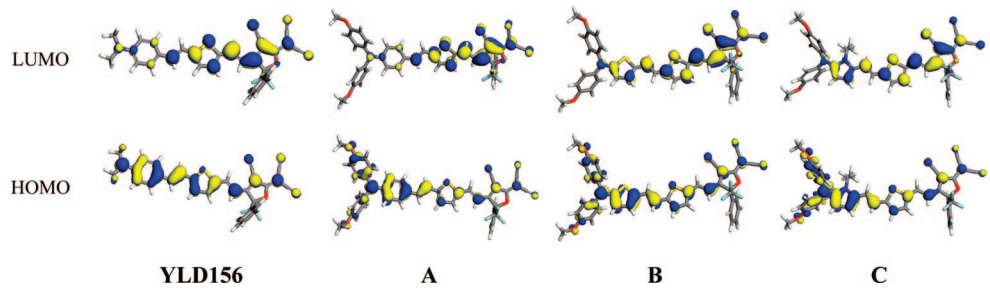

Figure 2. HOMO (bottom) and LUMO (top) surfaces of chromophores. Geometries were optimized with DMol[30,31] using PBE[32] functional with the *dnp* basis set under medium quality convergence criteria. Electrostatic moments and HOMO−LUMO energy gaps were calculated on the basis of these optimized geometries using Gaussian03[33] employing B3LYP[34] functional with 3-21G*[35,36] basis set (the pyrrole *n*-alkyl substituent was limited to an ethyl group for simplicity).

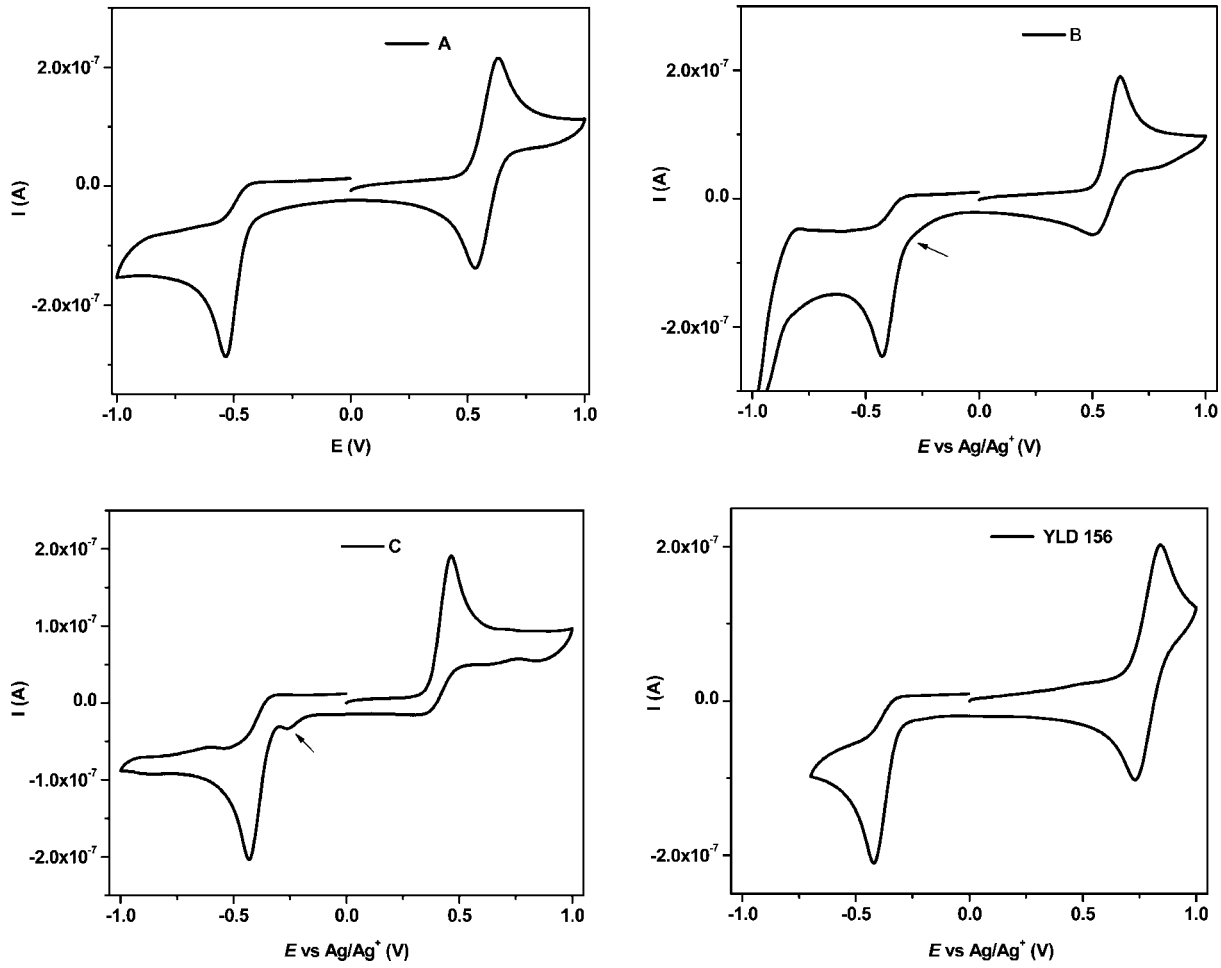

Figure 3. Cyclic voltammogram of chromophores recorded in CH_2Cl_2 with a scan rate of 50 mV/s using tetrabutylammonium hexafluorophosphate supporting electrolyte.

land on the donor, but instead reaches the acceptor. Following this, a chemical reaction probably occurs, making a neutral molecule that in turn accepts an electron from the electrode during the reduction cycle. The occurrence of a LUMO that is vastly delocalized from the heteroaryl part of the donor through the acceptor end is suggestive of this reactivity. It is possible that the oxidized species in these two cases possess lower LUMO energy than that of the neutral molecule. Evidence of this kind of chemical reaction may be noticeable just before the onset of the reductions of both compounds **B** (a shallow onset) and **C** (a small spike) close to 0.2 V relative to Fc.

The HOMO and LUMO energy levels were determined from the oxidation and reduction potentials, respectively. The ionization potential (IP) was calculated from the oxidation onset ($E_{\text{onset ox}}$) according to IP = $E_{\text{onset ox}}$ (Ag/Ag^+) + 4.8, where $E_{\text{onset ox}}$ (Ag/Ag^+) is the oxidation potential onset in volts versus the Ag/Ag^+ electrode. The LUMO energy level was similarly determined from the electron affinity (EA) from the reduction potential onset ($E_{\text{onset red}}$) according to IP = $E_{\text{onset red}}$ (SEC) + 4.4. The difference between these two values provides the HOMO − LUMO energy difference (ΔE (CV)). From the calculated values reported in Table 1, it can be concluded that the LUMO energy levels are approximately the same for all the compounds. Conversely, the HOMO energy levels are systematically lowered with an increase in the donor strength which influences the HOMO to a greater extent than the LUMO

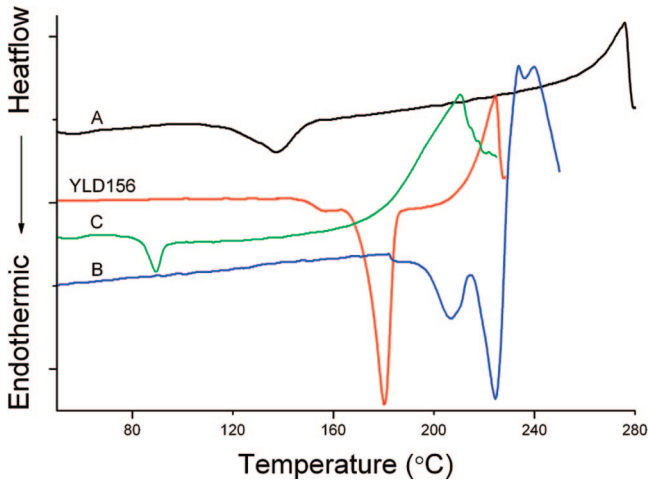

Figure 4. DSC thermograms of chromophores **A**, **B**, **C**, and **YLD156**.

Table 2. Thermal Properties

chromophore	T_g (°C)	T_d (°C)
YLD156	158	211
A	138	261
B	206	228
C	89	179

level. The electronic effect concomitant with the increased degree of conjugation moreover narrows the energy gap between the HOMO and the LUMO energy levels leading to ΔE values of 0.7 eV for **C**. The electrochemical values are corroborated by the spectroscopically measured values and also by the DFT calculations.

Trends in energy gaps between ΔE (optical) and ΔE (electrochemical) for the four compounds were found to be consistent. As is commonly observed, ΔE (optical) is significantly overestimated when compared to the data obtained by CV. The observed trends in optical and electrochemical ΔE support the idea that as the aromatic stabilization energy in the donor is reduced in moving from phenyl-, through thienyl-, to pyrrole-based donors, electron-donating strength is indeed enhanced. As ΔE is reduced, resulting in a bathochromic shift of λ_{max} within the series of compounds, it is noted that E_{red} remains very stable and E_{ox} is lowered.

Thermal Properties. Thermal properties of chromophores **A**, **B**, **C**, and **YLD156** were explored by differential scanning calorimetry and are shown and tabulated in Figure 4 and Table 2. Compounds **C**, **A**, **YLD156**, and **B** have a range of glass transition temperatures (T_g) of 89, 138, 158, and 206 °C, respectively. The relatively low T_g of **C** is likely due to the flexible hexyl chain on the pyrrole—molecular flexibility is known to reduce T_g. The thermal decomposition temperatures do not follow the same trends as T_g. **A** has by far the highest decomposition temperature (261 °C), followed by **B** (228 °C), **YLD156** (211 °C), and **C** (178 °C). These results are thought to be caused by two opposing effects. The enhanced thermal stability of the diarylamino donors (**A** and **B**) over the dialkylamino analogue, **YLD156**, is due to the absence of a sp^3 hybridized α-hydrogen adjacent to the donor nitrogen in the latter. This effect is partially offset by lower thermal stabilization of the thiophene and pyrrole moieties relative to the phenyl. Furthermore, T_d of **C** is likely further decreased due to the introduction of an α-hydrogen adjacent to the pyrrole nitrogen. Although the T_d of **C** is about 30 °C less than **YLD156**, it is still quite comparable to many commonly used chromophores like **AJC146** and **YLD124**.[9]

Nonlinear Optical Properties

Molecular nonlinearity. Molecular β_{ijk}, as described by quantum mechanical modeling, is usually reported as the nonlinear component of electron density polarization that is induced along the molecular dipolar axis when the molecule is acted upon by a static, DC (zero frequency) electric field [$\beta_{zzz}(0;0,0)$]. For dipolar chromophores, this is the largest component of the hyperpolarizability tensor.[37] Experimentally observed second-order nonlinear optical properties, such as second harmonic generation (SHG) and the electrooptic (EO) effect, often exhibit pronounced frequency dependence. This occurs when the frequency of the AC optical field approaches a molecular resonance. Therefore, when measured at a finite operational wavelength, λ_{exp}, the quantity that defines the electrooptic coefficient, r_{33}, is not zero frequency, $\beta_{zzz}(0;0,0)$, but is instead the frequency dependent $\beta_{zzz}(-\omega;0,\omega)$. For solution-based hyper-Rayleigh scattering measurements the important term is $\beta_{HRS}(-2\omega;\omega,\omega)$. For this reason, in order to compare chromophore systems having quite different values for ΔE_{eg}(optical) and thus different ω_{eg} in terms of DFT generated $\beta(0;0,0)$, frequency dispersion effects must be accounted for when analyzing experimental data. This deconvolution allows direct comparison of experimental measurements of r_{33} and $\beta_{HRS}(-2\omega;\omega,\omega)$ with quantum mechanical predictions of $\beta_{zzz}(0;0,0)$, made to correlate structural modification with enhancements in molecular nonlinearity.

In order to estimate the differences in frequency dependence among the chromophore series studied herein, the two-level model (TLM) may be employed. The simplified version of the TLM optical frequency dispersion formula needed for this study is taken from work by Singer, et al.[38] which can be written as

$$\beta_{ijk}(-\omega_3;\omega_1,\omega_2) = \frac{(3+\sqrt{r_1 r_2}-r_3)}{3\prod_{k=1}^{3}(1-r_k)}\beta_{ijk}(0;0,0) \qquad (1)$$

where the factor $r_\alpha = \omega_\alpha^2/\omega_o^2$, $1 \le \alpha \le 3$, is the square of the ratio of the radiation frequency, ω_α, to the frequency of the lowest-energy transition, $\omega_o = \Delta E/\hbar$. Converting to these ratios to wavelengths gives

$$\frac{\beta_{ijk}(-\omega;0,\omega)}{\beta_{ijk}(0;0,0)} = \frac{3-(\lambda_x/\lambda)^2}{3(1-(\lambda_x/\lambda)^2)^2} \qquad (2)$$

as appropriate for r_{33} and

$$\frac{\beta_{ijk}(-2\omega;\omega,\omega)}{\beta_{ijk}(0;0,0)} = \frac{1}{(1-(\lambda_x/\lambda)^2)(1-4(\lambda_x/\lambda)^2)} \qquad (3)$$

to be used with HRS. Here λ_x locates the absorption maximum, and λ is the excitation wavelength.

From the above relationships and the experimental values for λ_{max}, the frequency dependence of the nonlinear properties of each chromophore can be estimated.

Density functional theory (DFT) quantum mechanical methods were employed to determine theoretical values for the

(37) Cyvin, S. J.; Rauch, J. E.; Decius, J. C. *J. Chem. Phys.* **1965**, *43*, 4083–4095.
(38) Singer, K. D.; Kuzyk, M. G.; Sohn, J. E. *J. Opt. Soc. Am. B:* **1987**, *4*, 968–976.

Table 3. DFT Predictions of $\beta_{HRS}(0;0,0)$ and HRS Measurement Data Corrected by TLM

	theoretical data (DFT)		experimental data (HRS)			
cmpd	$\beta_{HRS}(0;0,0)$DFT	$\mu(D)$DFT	$\beta_{HRS}(-2\omega;\omega,\omega)$ exp. $\times 10^{-30}$esu	$\beta_{HRS}(-2\omega;\omega,\omega)/\beta_{HRS}(0;0,0)$ [a]	$\beta_{HRS}(-2\omega;\omega,\omega)$ corrected [b]	β_{HRS}(TLM) normalized [c]
YLD156	298	24	928 ± 106	3.19/2.31	672 ± 77	1
A	710	25	1129 ± 42	3.07/2.31	849 ± 31	1.26
B	660	25	2654 ± 209	6.74/2.31	909 ± 72	1.35
C	606	24	2334 ± 140	6.46/2.31	837 ± 50	1.24

[a] TLM proportionality factor derived using equation 3 divided by the TLM factor for the FTC standard; $TLM_{FTC} = 2.31(\lambda_x = 674nm)$. [b] β_{HRS} divided by TLM factor. [c] $\beta_{HRS}(corrected)/\beta_{HRS}(YLD156)$.

hyperpolarizability[39–41] for comparison with experiment. This data was then used to help correlate experimental measurements with structural effects as they are related to the electronic properties. Figure 2, depicts the electron density distribution of the HOMO and LUMO structures of the four chromophores. In addition to explaining the steady-state photophysical properties of the systems studied here, this illustration also demonstrates the substituent-induced ground- and excited-state electron density asymmetry along the dipolar axis of the chromophore that is essential for the induction of large $\beta_{zzz}(0;0,0)$ molecular nonlinearity.

Hyper-Rayleigh scattering (HRS) experiments were performed on chromophores **YLD156**, **A**, **B**, and **C**. The HRS technique unlike EFISH (electric field induced second harmonic generation), [42] allows direct evaluation of $\beta_{HRS}(-2\omega;\omega,\omega)$. The HRS measurements were performed using chloroform chromophore solutions at a fundamental wavelength of $\lambda_{exp} = 1.9$ μm, employing the Dalton group chromophore FTC [43–45] as an external standard.[46] The FTC reference value has been determined in house as; $\beta_{HRS}(-2\omega;\omega,\omega)$FTC = 445 ± 230. Because FTC also exhibits pronounced frequency dependence, using this standard allows the partial cancelation of the TLM factor, reducing the severity of this correction. Normalizing the resulting values against results for **YLD156**, and applying the proportionality factors derived using the TLM equation (eq 3), divided by $TLM_{FTC} = 2.31(\lambda_x = 674$ nm), we can compare hyperpolarizability values with those predicted by DFT. These data are presented in Table 3.

Using the TLM derived factor to estimate the expected frequency dependence, it is seen that although the exact magnitude of $\beta_{HRS}(0;0,0)$enhancement expected from theory may not be observed, experimental values compare quite favorably with DFT predictions considering measurement error. This also suggests that in this case, the simple TLM may be reasonably predictive. Within the **A**, **B**, and **C** chromophore series, $\beta_{HRS}(0;0,0)$values are found to be quite similar, in agreement with DFT. The discrepancy between absolute experimental and DFT $\beta_{HRS}(0;0,0)$, a factor of 2 to 3, is currently the subject of much interest. Since DFT modeling considers an isolated chromophore molecule in the gas phase, experimental measurements performed in chloroform solution are expected to be enhanced by a factor of this magnitude due to the reaction field of the solvent.

To advance the computer model one step beyond the simple TLM discussed above, the implications of the TLM can be combined with DFT in order to directly assess frequency dependence combined with reaction field calculations. In this manner, the TLM provides a means to estimate the frequency and solvent dependence of measurable properties of NLO molecules simultaneously. We illustrate the method here for molecule **C**, the pyrrole variant. According to Singer, et al.,[34] the frequency dependence of the hyperpolarizability (in atomic units) can be expanded as follows

$$\beta_{ijk}(-\omega_3;\omega_1,\omega_2) = \mathrm{sym}[\mu_{i;eg}\mu_{j;eg}(\mu_{k;ee} - \mu_{k;gg})]\frac{\omega_0^2(3\omega_0^2 + \omega_1\omega_2 - \omega_3^2)}{(\omega_0^2 - \omega_1^2)(\omega_0^2 - \omega_2^2)(\omega_0^2 - \omega_3^2)}$$

in the approximation that the perturbation series is dominated by just the one state above the ground state. Here sym[*] signifies symmetrization of all tensor components. The matrix element of the kth component of the dipole operator between states σ and ρ is denoted by $\mu_{k;\sigma\rho}$, the frequencies of the stimuli electric fields are ω_1 and ω_2, while the response frequency is $\omega_3 = \omega_1 + \omega_2$, and $\omega_0 = E_e - E_g$ is the energy gap between the ground and excited states in atomic units.

An ability to calculate excited-state dipole vectors, as well as transition moments, is available in the developmental version of Gaussian (GDV). We have used this functionality (with B3LYP and 3-21G*) to evaluate $\mu_{k;ee}$ as well as $\mu_{j;eg}$ for molecule **C**; the ground-state dipole $\mu_{k;gg}$ was done with Gaussian03. The advantage of the method is that all dipole matrix elements can be calculated concurrently with the PCM solvent calculation, which would be prohibitively expensive with the RT-TDDFT method described elsewhere.[45] Gaussian default parameters were used for the chloroform solvent. As shown in Figure 5, the results obtained using this method seem to be quite consistent with the uncorrected experimental values. Because this methods takes into account the dependence of $\beta_{HRS}(-2\omega;\omega,\omega)$ on both measurement frequency and dielectric (solvent) environment for each chromophore, the result should correspond to the uncorrected experimental results. Figure 5a illustrates that at $\lambda_{exp} = 1.9$ μm indeed the experimental value of $\beta_{HRS} = 928 \pm 106$ for **YLD156** compares quite favorably with the modified DFT predictions. Similar comparison of the experimental value for chromophore **C**, $\beta_{HRS} = 2334 \pm 140$, and Figure 5c, confirms that these values are also consistent.

Macroscopic Nonlinearity. Bulk material EO activity (r_{ij} coefficients) is governed by first nonlinear susceptibility, $\chi^{(2)}$. Realization of nonlinear susceptibility requires the removal of centrosymmetry both at the molecular and bulk levels. Provided

(39) Isborn, C. M.; Leclercq, A.; Vila, F. D.; Dalton, L. R.; Bredas, J. L.; Eichinger, B. E.; Robinson, B. H. *J. Phys. Chem. A* **2007**, *111*, 1319–1327.
(40) Kinnibrugh, T.; Bhattacharjee, S.; Sullivan, P.; Isborn, C.; Robinson, B. H.; Eichinger, B. E. *J. Phys. Chem. B* **2006**, *110*, 13512–13522.
(41) Liao, Y.; Eichinger, B. E.; Firestone, K. A.; Haller, M.; Luo, J.; Kaminsky, W.; Benedict, J. B.; Reid, P. J.; Jen, A. K. Y.; Dalton, L. R.; Robinson, B. H. *J. Am. Chem. Soc.* **2005**, *127*, 2758–2766.
(42) Teng, C. C.; Garito, A. F. *Phys. Rev. B.* **1983**, *28*, 6766.
(43) Dalton, L. R.; Harper, A.; Ren, A.; Wang, F.; Todorova, G.; Chen, J.; Zhang, C.; Lee, M. *Ind. Eng. Chem. Res.* **1999**, *38*, 8.
(44) Kaatz, P.; Shelton, D. P. *Opt. Commun.* **1998**, *157*, 177–198.
(45) Takimoto, Y.; Vila, F. D.; Rehr, J. J. *J. Chem. Phys.* **2007**, *127*, 154114.
(46) Akelaitis, A. J. P.; Olbricht, B. C.; Sullivan, P. A.; Liao, Y.; Lee, S. K.; Bale, D. H.; Lao, D. B.; Kamisky, W.; Eichinger, B. E.; Choi, D. H.; Dalton, L. R. *Opt. Mater.* **2007**, ; http/dx.doi.org/10.1016/j.optmat.2007.09.007.

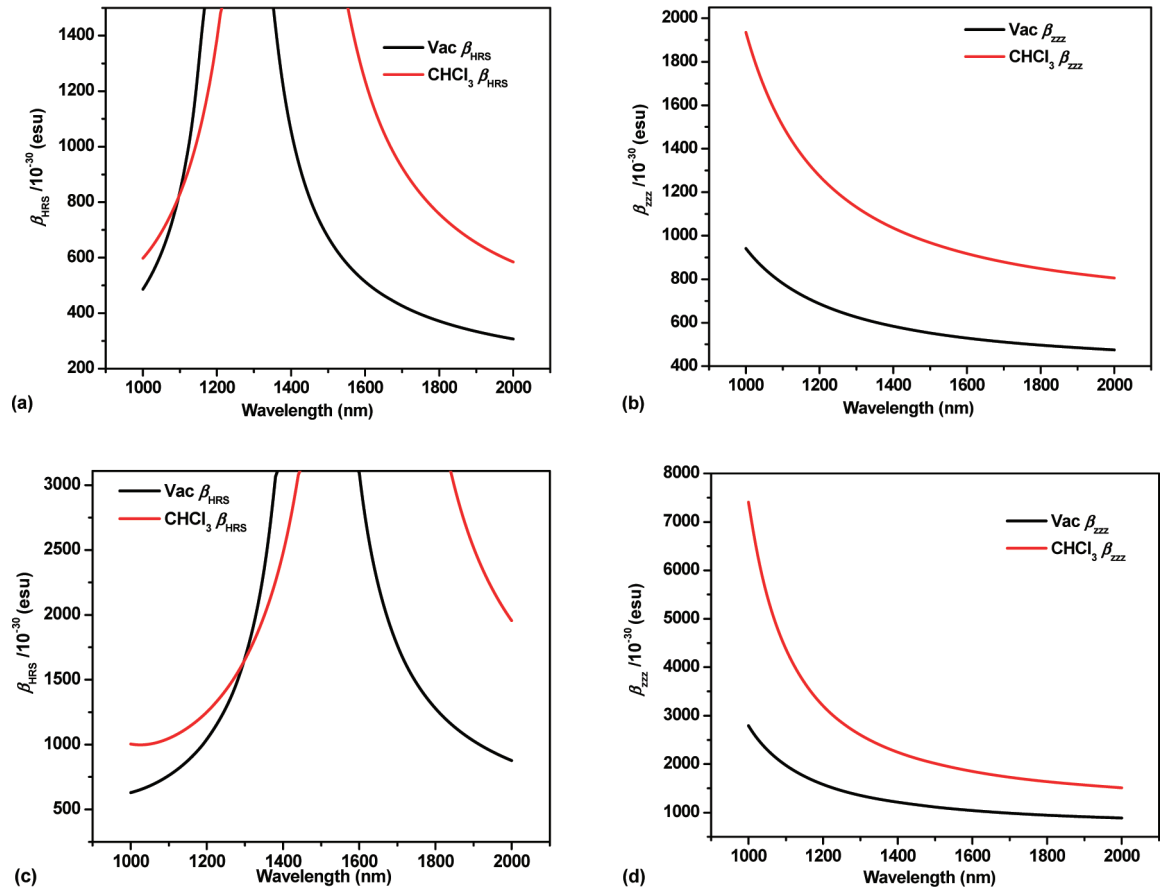

Figure 5. Plots of calculated molecular hyperpolarizabilities in vacuum and in the presence of solvent ($CHCl_3$) showing frequency dependence: (a) and (b) of **YLD 156**; (c) and (d) of chromophore **C**.

that the molecular hyperpolarizability tensor is dominated by the component that is oriented along the dipolar molecular axis, β_{zzz}, the first nonlinear susceptibility may be described by the relation

$$\chi^{(2)}_{zzz} = N\beta_{zzz}(-\omega;0,\omega)\langle\cos^3\theta\rangle g(\omega) \quad (4)$$

where N represents chromophore number density, θ is the angle between the chromophore dipolar axis and the poling vector, and $\langle\cos^3\theta\rangle$ is the acentric order parameter. The term, $g(\omega)$, denotes the Lorentz−Onsager local field factors. For the materials considered herein, $g(\omega)$, should only differ by no more than ±10% from system to system, and will be neglected for the sake of simplicity.[38] The Pockels tensor component, r_{33}, of interest to device performance is related to $\chi^{(2)}$by

$$r_{33} = -2\chi^{(2)}/n^4 \quad (5)$$

in which n is the refractive index of the material at the operational wavelength.

To complete the analysis presented herein, two complementary experimental techniques were used for evaluation of nonlinear optical behavior. A Teng−Man technique reflection ellipsometry apparatus (TMT), modified to perform real-time monitoring of electrooptic activity, was used to optimize poling conditions and perform initial r_{33} measurements.[47] In order to obtain r_{33} data at two different wavelengths (λ_{exp} = 1310 nm and λ_{exp} = 1550 nm), and to provide an alternate r_{33} measurement for comparison, the ATR technique was modified to accommodate high-refractive index polymers through the use of a rutile prism. The same sample format that is used for the TMT measurement is also employed for ATR. In this report samples were taken directly from poling and measurement, using the *in situ* TMT, to a supplementary measurement on the ATR setup. The ATR technique is a modification of the widely used prism-coupling refractive index measurement.[48]

A change in the prism-coupling angle, due to the electrooptic effect, is measured by monitoring the change in intensity of the laser light reflected from the prism/sample interface as a function of applied voltage. A schematic representation of the experimental apparatus is shown in Figure 6. The sample is mounted on the prism using a pneumatic plunger. The plunger, prism, and detector are mounted atop a stepper motor to allow precise control over the incidence angle of the measurement laser. The electrooptic coefficient, r_{33}, is calculated using the relation

$$r_{33} = \frac{2d\Delta R}{n_{TM}^3 V}\frac{\delta n_{eff}}{\delta\theta}\Big/\left(\frac{\delta R}{\delta\theta}\frac{\delta n_{eff}}{\delta n_{TM}}\right) \quad (6)$$

where d is the thickness of the polymer film and n_{TM} is the film refractive index. As the sample is rotated past the coupling angle, the intensity of the DC reflected signal, R, is recorded. Simultaneously, the change in R, related to the change in

(47) Sullivan, P. A.; Olbricht, B. C.; Akelaitis, A. J. P.; Mistry, A. A.; Liao, Y.; Dalton, L. R. *J. Mater. Chem.* **2007**, *17*, 2899–2903.

(48) Chen, A.; Chuyanov, V.; Garner, S.; Steier, W. H.; Dalton, L. R. *Organic Thin Films for Photonics Applications, OSA Technical Digest Series*; 1997; Vol. 14, pp 158−160.

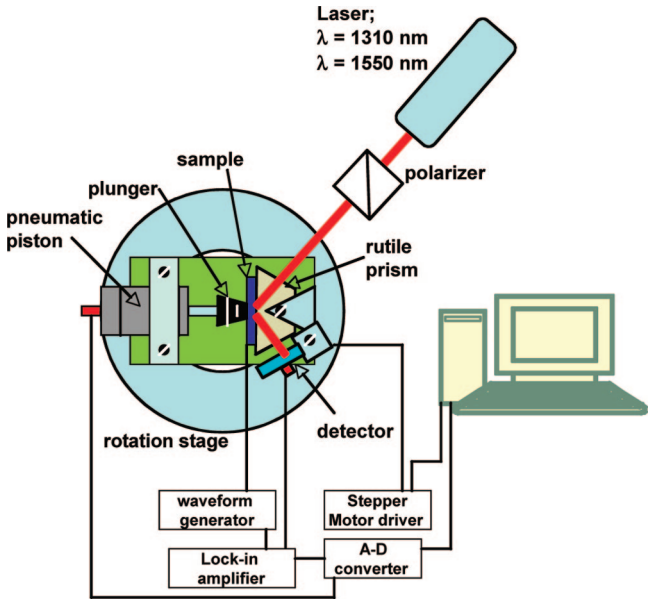

Figure 6. Schematic representation of the attenuated total reflection (ATR) electrooptic coefficient measurement apparatus modified to use a high index rutile prism, operating at $\lambda_{exp} = 1310$ nm and $\lambda_{exp} = 1550$ nm.

refractive index caused by application of an AC modulation voltage, V, is recorded using a lock-in amplifier. Here, $n_{eff} = n_p \sin\theta$ where n_p is the prism refractive index. Rutile TiO_2 has a refractive index of $n_o(1310\text{ nm}) = 2.462$ and $n_o(1550\text{ nm}) = 2.453$. The current setup includes two laser sources for measurement of r_{33} at $\lambda_{exp} = 1310$ nm and $\lambda_{exp} = 1550$ nm for the purpose of determining poling efficiency, r_{33}/E_p, as a function of measurement wavelength. From eqs 4 and 5, assuming the order produced by poling, $\langle\cos^3\theta\rangle/E_p$, chromophore number density, N, and refractive index, n_{TM}, are the same in all samples, it follows that any difference in r_{33}/E_p between $\lambda_{exp} = 1310$ nm and $\lambda_{exp} = 1550$ nm must be due to the dependence of $\beta_{zzz}(-\omega;0,\omega)$ on measurement wavelength. This difference should be well approximated using the proportionality factor obtained from applying the TLM, eq 2. Performing this experiment during evaluation of the chromophores under study provides a simple but valuable check on the applicability of the TLM.

Shown in Figure 7 is r_{33} data corresponding to chromophore **B**, as measured by ATR at both wavelengths, plotted as a function of poling voltage. The error shown is the standard error of the fit. The slope of this plot is the poling efficiency, $r_{33}/E_p(\text{nm/V})^2$. From eq 4, using λ_{max} ($CHCl_3$) = 753 nm, the difference in $\beta_{zzz}(-\omega;0,\omega)$ between $\lambda_{exp} = 1310$ nm and $\lambda_{exp} = 1550$ nm is predicted to be $(1.41)[\beta_{zzz}\ (1550\text{ nm})] \approx [\beta_{zzz}(1310\text{ nm})]$ by the TLM approximation. Measured experimentally, $(1.5)[r_{33}/E_p\ (1550\text{ nm})] = [r_{33}/E_p\ (1310\text{ nm})]$. Holding all other quantities equal, an assumption that should be valid for the case where the values at both wavelengths are measured on the same samples by simply changing laser sources, it is suggested that the TLM is reasonably predictive. Similar analyses were performed for chromophores **YLD156** and **A**. Consistent results were again obtained.

Table 4 lists the results obtained through the TMT technique and ATR for chromophores **B** and **C**. Also listed are the previously reported TMT results corresponding to chromophores **YLD156** and **A**, along with the corresponding TLM proportionality factors. In this case, the TLM factors for $\beta_{zzz}(-\omega;0,\omega)/\beta_{zzz}(0;0,0)$ are normalized to chromophore **YLD156** to aid in

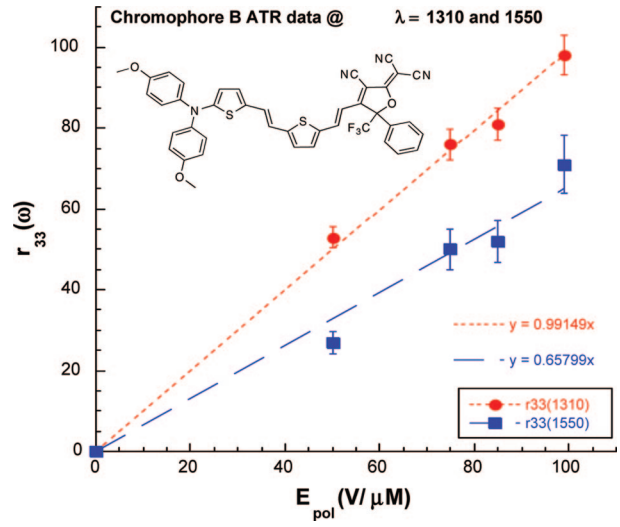

Figure 7. Plot of the ATR measurement data taken for a series of samples poled using increasing E_p of chromophore **B** loaded into APC at 25% by weight.

Table 4. Comparison of the Calculated and the Experimental Nonlinear Properties with Order Measurements

cmpd	$\beta_{zzz}(0) \times 10^{-30}$ esu (DFT)[a]	r_{33}/E_{pol} (nm/V)^2 (Teng−Man)[b]	r_{33}/E_{pol} (nm/V)^2 (ATR)[c] 1310 nm	1550 nm	TLM factor[d]	$\langle P_2\rangle/E_{pol}$[e]
YLD156	340	0.44[b]	0.42	0.35	1	0.00041
A	715	0.60[b]	0.36	0.28	0.98	0.00012
B	631	1.11	0.99	0.66	1.32	–
C	606	1.21	1.24	–	1.30	0.00046

[a] $\beta_{zzz}(0;0,0)$calculated by DFT. [b] Literature value measured by TMT. [c] r_{33}/E_p values measured by ATR. [d] TLM factors normalized against **YLD156**; TLM(chrom)/TLM(YL156). [e] Centrosymmetric order parameter as a function of poling field measured by VAPAS.

the simplicity of the comparison among chromophores. Also tabulated are DFT values for β_{zzz} (0;0,0), and centrosymmetric order parameter measurements, $\langle P_2\rangle/E_p$.

When different samples composed of different materials are compared, it may not be sufficient to assume that $\langle\cos^3\theta\rangle/E_p$ is the same or even comparable. If the order induced by poling is indeed very different, comparison of $\beta_{zzz}(0;0,0)$ between materials based on r_{33}/E_p and TLM factors will be rendered unhelpful without direct comparison of polar order. No direct measurement of dipolar order is known. However, the centrosymmetric order parameter $\langle P^2\rangle = 1/2(3\langle\cos^2\theta\rangle - 1)$ may be evaluated though simple linear dichroism measurements using the ratio variable angle polarized absorption spectroscopy method.[49,50] These measurements were performed for poled samples of the chromophores under study here to gain information about possible differences in poling induced order between materials. Analogous to r_{33} data, $\langle P^2\rangle$was evaluated for a number of poled samples and plotted as a function of poling voltage for each material. In this manner poling induced dichroism, $\langle P_2\rangle/E_p$, can be compared among the chromophores. This data is also listed in the last column of Table 4.

Finally, with measurements of r_{33}/E_p, $\langle P_2\rangle/E_p$, and TLM frequency correction factors, we are ready to make qualitative

(49) Graf, H. M.; Zobel, O.; East, A. J.; Haarer, D. *J. Appl. Phys.* **1994**, *75*, 3335–3339.
(50) Rommel, H. L.; Robinson, B. H. *J. Phys. Chem. C* **2007**, *111*, 18765–18777.

comparisons of intrinsic hyperpolarizability as predicted by DFT within a group of structurally similar, but electronically dissimilar, EO chromophores. For example, $\beta_{zzz}(0;0,0)$ predicted by DFT calculations can be compared with experimental results using the relation

$$\frac{\dfrac{r_{33}}{E_p}(\text{chrom})}{\left\{\left[\dfrac{\beta_{zzz}(0)(\text{chrom})}{\beta_{zzz}(0)(\text{YLD156})}\right][\text{TLMfactor}]\left[\dfrac{\langle p_2\rangle/E_p(\text{chrom})}{\langle p_2\rangle/E_p(\text{YLD156})}\right]\right\}} \approx \frac{r_{33}}{E_p}(\text{YLD156}) \quad (7)$$

Substituting the data from Table 4 into eq 7, we can evaluate the agreement between DFT and experiment for chromophore **C** as follows:

$$\frac{1.24}{\left\{\left(\dfrac{606}{340}\right)(1.30)\left(\dfrac{0.00046}{0.00041}\right)\right\}} = 0.48 \quad (8)$$

This comparison also yields quite good agreement when applied to the remaining chromophore results. Such a good agreement suggests that DFT calculations are reasonably predictive of trends in r_{33} when the frequency dependence of nonlinear effects is accounted for and poling-induced order can be estimated. Applying the above qualitative relation, the argument can be supported that dianisyl donor-based chromophores **A**, **B**, and **C** indeed deliver $\beta_{zzz}(0;0,0)$values that are enhanced by as much as a factor of 2, as predicted by DFT, compared to the **YLD156** chromophore standard. Chromophore **B**, with its relatively rigid and overall planar structure, does not respond well to the poling field, showing a low value for $\langle P_2\rangle/E_p$compared to the other chromophores in the series. The data above suggests that even though chromphore **B** should possess almost double the $\beta_{zzz}(-\omega;0,\omega)$ of **YLD156**, the acentric order produced by poling is only half as large, resulting in a cancelation of effects and a very similar r_{33}/E_p. Such poor poling induced ordering behavior may be explained by differences in chromophore-host compatibility and chromophore shape.[50] Therefore, in order to realize improvements in r_{33}/E_p such factors must be taken into account in addition to hyperpolarizability as illustrated in the recent work by Cheng et al.[9]

Conclusions

Two new theory-inspired, highly hyperpolarizable chromophores, based on the bis-(4-methoxyphenyl)*hetero*-aryl-amino donor (thiophene and *N*-hexylpyrrole) with 2,5-divinylenethienyl bridges, and CF_3-Ph-TCF acceptors have been synthesized. Efficient synthetic approaches were developed to reach these heteroaryl-amino donors. In addition to recording thermal, electrochemical, and analytical data, linear and nonlinear optical (NLO) properties were thoroughly investigated for all compounds. The newly prepared dianisylaminothienyl and dianisylaminopyrrolyl chromophores both show nearly a 3-fold enhancement in EO activity as compared to the previously reported dianisylaminophenyl analogues.

Several optical effects contribute to enhanced, poling-induced, electrooptic activity. Evaluation of the absorption spectra within the compound series revealed that as the donor is systematically modified from dialkyl (**YLD156**), and diaryl (**A**), to diaryl thiophene (**B**), and diarylpyrrole (**C**), a significant reduction in ΔE_{eg} is observed. Electrochemical data confirmed that the oxidation potentials of the heteroaromatic donor chromophores are significantly reduced, supporting the argument that such modification indeed enhances electron-donor strength and is the major cause of the reduced optical ΔE_{eg}.

Modeling of the nonlinear optical properties of the chromophore structures reveals that when the dialkyl-substituted amine donor is replaced by a di-*p*-methoxyphenyl-substituted amine, a factor of approximately twice enhancement in $\beta(0;0,0)$can be expected regardless of the nature of the central donor aromatic ring. However, simple analysis of these predictions was not sufficient for the purpose of rationalizing experimental differences in r_{33} and $\beta_{HRS}(-2\omega;\omega,\omega)$, as correlated with molecular structure modification.

Chemical alteration of the fundamental chromophore structure results in pronounced variation in the optical ΔE_{eg}, molecular shape, and solubility characteristics, as well as other complicating factors that must be addressed in order for chromophores to be intercompared. In the case of HRS evaluation of $\beta_{HRS}(-2\omega;\omega,\omega)$, measurement frequency (excitation wavelength) dependence of molecular nonlinearity must be taken into account. In this report it is shown that the simple two-level model, in which HOMO and LUMO level contributions are assumed to dominate the relevant molecular electronic properties, is relatively satisfactory for this purpose. Correction of experimental data using the TLM approximation results in good agreement between theory and experiment. To extend this TLM-based frequency dependence analysis to solid-state electrooptic activity, the applicability of the TLM was confirmed by r_{33} measurements at multiple wavelengths using a newly modified ATR experiment. For comparison of r_{33} measurements with quantum mechanical predictions, experimental evaluation of poling induced order was also required. Using a variable angle polarized absorption spectroscopy technique, also modified in our laboratories, $\langle P_2\rangle/E_p$ was evaluated. The ratio $\langle P_2\rangle/E_p$ is found to correlate directly with the ratio r_{33}/E_p. Combining DFT and TLM predictions with $\langle P_2\rangle/E_p$ measurements, systematic donor modification has been successfully correlated with changes in poling induced r_{33}. This study emphasizes the need for simultaneous consideration of many interrelated effects resulting from seemingly straightforward chromophore modification. Molecular structure must be optimized not only for hyperpolarizability, but also for chromophore shape and solubility. Combined theoretical analysis and thorough experimental characterization of systematically modified materials allows the continued development of improved electrooptic materials through a heightened understanding of increasingly detailed structure−property relationships.

Experimental Section

Complete synthetic details of all compounds and characterization details are available in the Supporting Information.

Acknowledgment. We acknowledge the support of the STC-MDITR Program of the National Science Foundation (DMR0120967) and NSF-(DMR-0092380). Support from the DARPA MORPH Program Phase II ((N) 14-04-10094), is also gratefully acknowledged.

Supporting Information Available: Experimental methods, procedures for the synthesis of new compounds, complete characterization data, and complete ref 33. This material is available free of charge via the Internet at http://pubs.acs.org.

JA8007424